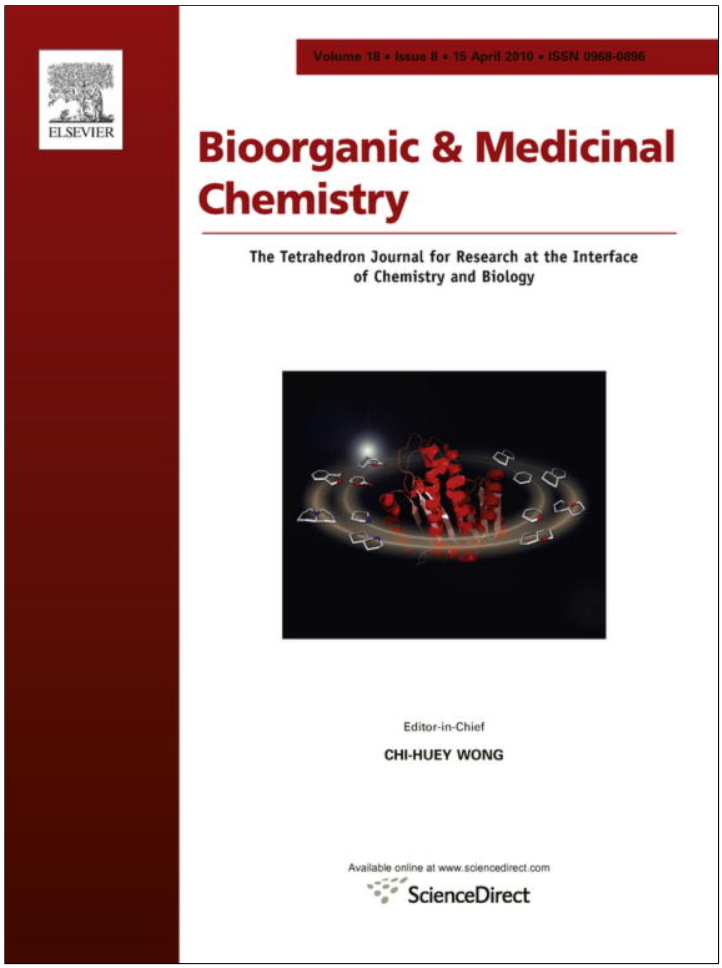

Bioorganic & Medicinal Chemistry 18 (2010) 2912–2919

Contents lists available at ScienceDirect

Bioorganic & Medicinal Chemistry

journal homepage: www.elsevier.com/locate/bmc

Ircinialactams: Subunit-selective glycine receptor modulators from Australian sponges of the family Irciniidae

Walter Balansa [a], Robiul Islam [b], Frank Fontaine [a], Andrew M. Piggott [a], Hua Zhang [a], Timothy I. Webb [b], Daniel F. Gilbert [b], Joseph W. Lynch [b], Robert J. Capon [a,*]

[a] Institute for Molecular Bioscience, The University of Queensland, St. Lucia, QLD 4072, Australia
[b] Queensland Brain Institute and School of Biomedical Sciences, The University of Queensland, St. Lucia, QLD 4072, Australia

ARTICLE INFO

Article history:
Received 8 February 2010
Revised 2 March 2010
Accepted 3 March 2010
Available online 6 March 2010

Keywords:
Glycine receptor (GlyR) chloride channels
Glycinyl lactam sesterterpenes
Marine natural products
Ircinidae

ABSTRACT

Screening an extract library of >2500 southern Australian and Antarctic marine invertebrates and algae for modulators of glycine receptor (GlyR) chloride channels identified three Ircinidae sponges that yielded new examples of a rare class of glycinyl lactam sesterterpene, ircinialactam A, 8-hydroxyircinialactam A, 8-hydroxyircinialactam B, ircinialactam C, *ent*-ircinialactam C and ircinialactam D. Structure–activity relationship (SAR) investigations revealed a new pharmacophore with potent and subunit selective modulatory properties against α1 and α3 GlyR isoforms. Such GlyR modulators have potential application as pharmacological tools, and as leads for the development of GlyR targeting therapeutics to treat chronic inflammatory pain, epilepsy, spasticity and hyperekplexia.

1. Introduction

Glycine-gated chloride channel receptors (GlyRs) play a pivotal role in orchestrating inhibitory neurotransmission in the central nervous system.[1] Although they are generally known to be concentrated at the post-synaptic densities of neurons in the spinal cord, brainstem and retina, GlyRs are also located pre-synaptically at several synapses.[2–4] GlyRs are members of the Cys-loop ion channel receptor family and comprise a family of five subunits, α1–α4 and β. Functional GlyRs can be formed either as pentameric α subunit homomers or as αβ subunit heteromers.[1,5] The α1–α4 subunits exhibit differential central nervous system distribution patterns that are particularly evident in the superficial dorsal horn of the spinal cord,[6] and the retina.[7–9] On the other hand, the β subunit is broadly distributed throughout the brain. The physiological consequences of the differential α subunit distribution patterns are difficult to establish, as there are currently few pharmacological probes that can selectively inhibit specific GlyR isoforms.[10,11] Although several synthetic cannabinoid agonists (e.g., HU-210, HU-308 and WIN-55,212-2) effect a strong pharmacological discrimination between α1-containing and α3-containing GlyRs,[12] these ligands are generally unsuitable for physiological or behavioural studies due to non-specific actions at cannabinoid receptors CB1 and CB2. As such, small molecule subunit selective modulators of GlyRs would have significant value as pharmacological tools.

A further reason for identifying novel GlyR subunit-specific ligands is to identify therapeutic lead compounds for muscle relaxation, inflammatory pain, immunomodulation and epilepsy. As α1β GlyRs mediate inhibitory neurotransmission onto spinal motor neurons,[1] increasing α1β GlyR activity dampens motor neuron activity and hence reduces muscle contractility. Although generally sparsely distributed, the α3 subunit is strongly expressed in glycinergic synapses on nociceptive sensory neurons in the superficial layers of the spinal cord dorsal horn.[6] A variety of evidence[13] indicates that inflammatory pain sensitisation is caused by a prostaglandin E2-mediated down-regulation of α3-mediated glycinergic inhibitory currents in nociceptive neurons. This could produce 'disinhibition' of nociceptive projection neurons, resulting in the increased transmission of pain impulses to the brain, thereby explaining inflammatory pain sensitisation. Agents that restore (i.e., potentiate) glycinergic currents could therefore have potential as analgesics for chronic inflammatory pain. Although α1 is also expressed in nociceptive neurons, the α3 GlyR is considered a more promising therapeutic target as its sparse distribution outside the dorsal horn implies a reduced risk of side-effects.[11,13,14]

Functional GlyRs are also present in a variety of immune cells, including macrophages and leucocytes, where they are thought to mediate the anti-inflammatory effects of glycine.[15,16] Thus, the systemic administration of enhancing agents specific for α1- or α2-containing GlyRs could limit the damage inflicted by the inflammatory immune response on essential biological molecules, cells and organs. Finally, RNA-edited high-affinity transcripts of α2 and α3 GlyRs are upregulated in human temporal lobe epilepsy

* Corresponding author. Tel.: +61 7 3346 2979; fax: +61 7 3346 2090.
E-mail address: r.capon@imb.uq.edu.au (R.J. Capon).

0968-0896/$ - see front matter © 2010 Elsevier Ltd. All rights reserved.
doi:10.1016/j.bmc.2010.03.002

and there is evidence for a causative relationship between this upregulation and the condition.[17,18] Thus, antagonists selective for high-affinity α2- or α3-containing GlyRs may be useful for treating this chronic and debilitating neurological disorder. Considering all this information, it would be potentially useful to identify novel compounds with potent and specific potentiating or inhibitory effects on any individual GlyR isoform.

The aim of this study was to identify novel GlyR subunit-specific modulators from marine natural products with potential either as therapeutic leads or as pharmacological probes for unravelling glycinergic mechanisms in the central nervous system and immune system.

2. Results

2.1. Fluorescence-based screening

A collection of >2500 southern Australian and Antarctic marine invertebrates and algae were initially screened against recombinantly expressed α1 and α3 GlyRs using a yellow fluorescent protein (YFP)-based anion influx assay as described in Section 5. While the fluorescence assay employed was robust, some problems associated with autofluorescence of the extracts were encountered. These problems were largely overcome by using cell selection masks during quantitative microscopy to only measure fluorescence specifically associated with cell cytoplasms. In addition, some extracts resulted in false positives due to disruption of cellular membranes and leakage of YFP. Consequently, the cellular morphology in all active wells had to be assessed to ensure membrane integrity had been maintained. Finally, all active fractions were subjected to a second round of screening, yielding 27 marine extracts with confirmed antagonistic activity.

2.2. Isolation and structure elucidation

Chemical investigation of active extracts derived from three sponges of the Family Ircinidae yielded the known sponge metabolites (7*E*,12*E*,20*Z*,18*S*)-variabilin (**1**), (7*E*,12*Z*,20*Z*,18*S*)-variabilin (**2**) and (12*E*,20*Z*,18*S*)-8-hydroxyvariabilin (**3**), along with new examples of a rare class of glycinyl lactam sesterterpenes, ircinialactam A (**4**), 8-hydroxyircinialactam A (**5**), 8-hydroxyircinialactam B (**6**), ircinialactam C (**7**), *ent*-ircinialactam C (**8**) and ircinialactam D (**9**) (Scheme 1). All these metabolites belong to a common biosynthetic family, collectively known as sesterterpene tetronic acids, with the archetypal example being **1**. It is noteworthy that the ircinialactams were present at 10–100-fold lower concentrations in the sponge extracts than the corresponding variabilins, necessitating the use of HPLC–SPE–NMR for structure elucidation.

(7*E*,12*E*,20*Z*,18*S*)-Variabilin (**1**) was first reported from the marine sponge *Ircinia variabilis* in 1973,[19] and its full stereostructure described in 1994.[20] Over the last 25+ years several dozen variabilins have been reported, featuring differing levels of oxidation, stereochemistry and double bond regiochemistry. These include **2** from a Maltese *Ircinia oros*[21] and **3** from a New Zealand *Sarcotragus* sp.[22] Samples of **1**–**3** recovered during this current investigation were identified by spectroscopic analysis, with configurations

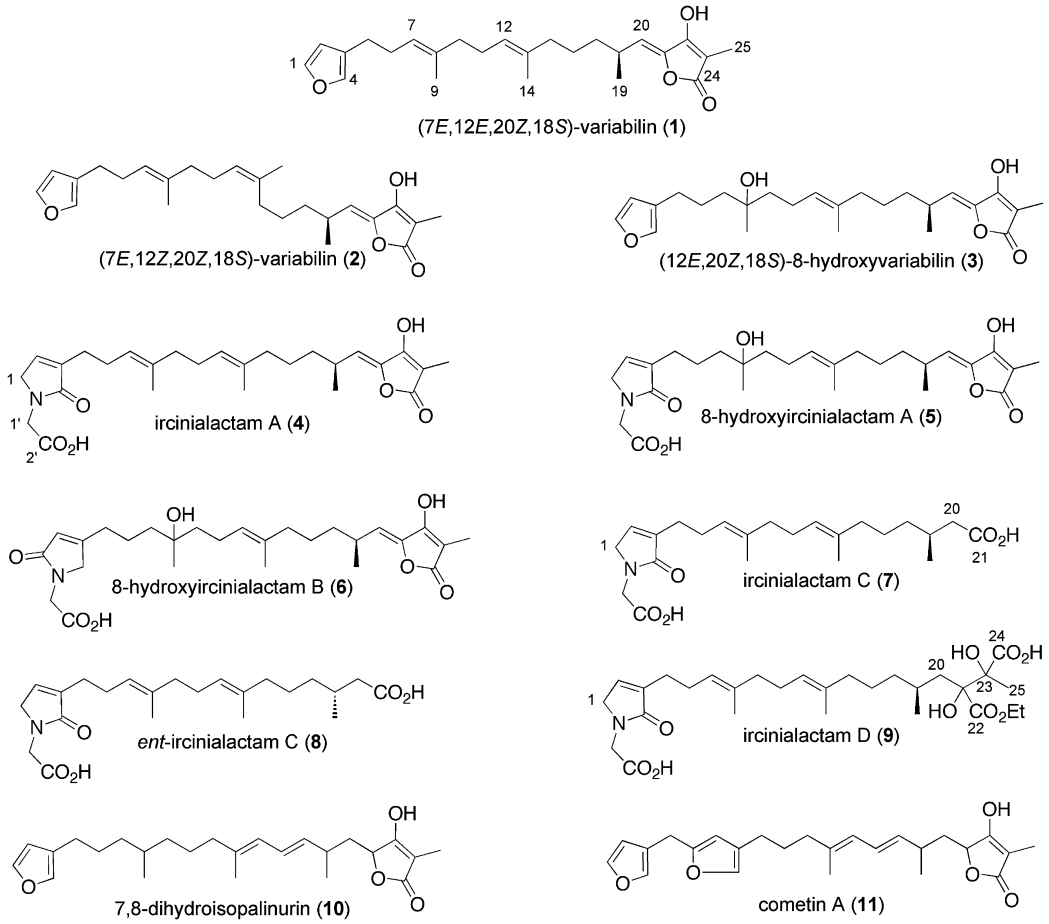

Scheme 1. Marine natural products investigated for GlyR modulating properties.

about $\Delta^{7,8}$ and $\Delta^{12,13}$ defined by the ^{13}C NMR chemical shifts for the corresponding olefinic methyls (E ~16 ppm, Z ~23 ppm), and configuration about $\Delta^{20,21}$ defined by the ^{13}C NMR chemical shift for C-20 (E ~121 ppm, Z ~117 ppm).[22] Double bond regiochemistry was determined from 2D NMR correlations, and absolute configuration by $[\alpha]_D$ measurements[20,22–24] and biogenetic considerations. Full 1D and 2D NMR (methanol-d_4) data for **1**–**3** are presented in the Supplementary data.

The remaining metabolites **4**–**9** are noteworthy in that the precursor furan moiety has undergone modification to the rare glycinyl lactam functionality. Such sesterterpene glycinyl lactams are a relatively recent addition to the scientific literature, having been described from Korean *Sarcotragus* spp.[25–27] Diagnostic NMR resonances consistent with conversion of a furanyl to a glycinyl lactam include replacement of α-furan methines (H-1 and H-4) with resonances for glycinyl (1′-H_2, δ_H ~4.2) and lactam (1-H_2 or 4-H_2 δ_H ~4.0) methylenes, and the appearance of a lactam carbonyl (C-4 or C-1, δ_C ~174).[26] The ^1H NMR chemical shift for H-2 is also diagnostic of lactam regiochemistry, (1-H_2, δ_H ~6.8; 4-H_2, δ_H ~5.8).[26] Metabolites **7**–**8** are glycinyl lactams further modified by biosynthetic truncation of the carbon skeleton (C_{25}–C_{21}) with concomitant transformation of the tetronic acid to a carboxylic acid. Such C_{21} furanoterpenes have been reported as co-metabolites with sesterterpene tetronic acids from a Spanish *Ircinia* sp.,[28] as well as both New Zealand[22] and Korean[27] *Sarcotragus* spp. Metabolite **9** is a glycinyl lactam further modified by ring opening and rearrangement of the tetronic acid functionality, to return a distinctive dihydroxy diacid (ester) terminus. The first reported examples of such a dihydroxy diacid (as the dimethyl ester) appeared as recently as 2008, as co-metabolites with sesterterpene tetronic acids from a Korean *Sarcotragus* sp.[27] A more detailed account of the structure proofs of **4**–**9** is presented below.

(+)HRESIMS analysis of ircinialactam A (**4**) returned a pseudomolecular ion $[M+Na]^+$ consistent with a molecular formula ($C_{27}H_{37}NO_6$, Δmmu 0.5) requiring ten double bond equivalents (DBE) and indicative of a glycinyl lactam analog of **1**. Analysis of the NMR data (Table 1) revealed diagnostic resonances for configurations about $\Delta^{7,8}$ (C-9, δ_C 16.0, E), $\Delta^{12,13}$ (C-14, δ_C 15.9, E) and $\Delta^{20,21}$ (C-20, δ_C 115.9, Z), and the glycinyl lactam regiochemistry (H-2, δ_H 6.88). Excellent correlations between the ^{13}C NMR data for **4** with that of **1**, particularly across the C-12 to C-25 structure fragment, together with analysis of the complete 1D and 2D NMR data and a −ve $[\alpha]_D$, supported the assigned structure.

(+)HRESIMS analysis of 8-hydroxyircinialactam A (**5**) returned a pseudomolecular ion $[M+Na]^+$ consistent with a molecular formula ($C_{27}H_{39}NO_7$, Δmmu 0.6) requiring nine DBE and indicative of a glycinyl lactam analog of **3**. Analysis of the NMR data (Table 2) revealed diagnostic resonances for configurations about $\Delta^{12,13}$ (C-14, δ_C 15.7, E) and $\Delta^{20,21}$ (C-20, δ_C 115.7, Z), and the glycinyl lactam regiochemistry (H-2, δ_H 6.93). Excellent correlations between the ^{13}C NMR (methanol-d_4) data for **5** with that of **3**, particularly across the C-12 to C-25 structure fragment, together with analysis of the complete 1D and 2D NMR data and a −ve $[\alpha]_D$, supported the assigned structure. The configuration about C-8 remains unassigned. The isomeric co-metabolite 8-hydroxyircinialactam B (**6**) displayed excellent NMR comparisons to **5**, with resonances diagnostic for configurations about $\Delta^{12,13}$ (C-14, δ_C 15.7, E) and $\Delta^{20,21}$ (C-20, δ_C 115.8, Z), and for the alternative glycinyl lactam regiochemistry (H-2, δ_H 5.88). Analysis of the complete 1D and 2D NMR data (Table S4, Supplementary data) and a −ve $[\alpha]_D$, supported the assigned structure.

(+)HRESIMS analysis of ircinialactam C (**7**) returned a pseudomolecular ion $[M+Na]^+$ consistent with a molecular formula ($C_{23}H_{35}NO_5$, Δmmu 0.6) requiring seven DBE, suggestive of the glycinyl lactam of C_{21} furanoterpene analogue of **1**. Analysis of the NMR data (Table 3) revealed diagnostic resonances for configurations about $\Delta^{7,8}$ (C-9, δ_C 16.1, E) and $\Delta^{12,13}$ (C-14, δ_C 15.9, E), and the glycinyl lactam regiochemistry (H-2, δ_H 6.89). Excellent correlations between ^{13}C NMR data for **7** and **4**, particularly across the C-1 to C-19 structure fragment, together with analysis of the complete 1D and 2D NMR data and a −ve $[\alpha]_D$, supported the assigned

Table 1
NMR data (600 MHz, methanol-d_4) for ircinialactam A (**4**)

#	δ_H (mult, J Hz)	δ_C[a]	COSY	HMBC (^1H–^{13}C)
1	4.05 (br s)	52.9	2	2, 3
2	6.88 (br s)	138.7	1	1, 4
3		139.2		
4		174.2		
5	2.28[b]	26.8		3, 6
6	2.26[b]	27.0	7	3, 5, 7, 8
7	5.14 (br t, 6.5)	124.5	6	5, 9, 10
8		137.2		
9	1.59 (br s)	16.0		7, 8, 10
10	1.99 (t, 7.3)	40.7	11	8, 9, 11, 12
11	2.08 (m)	27.4	10, 12	10, 12, 13
12	5.10 (br t, 6.5)	125.6	11	11, 14, 15
13		135.9		
14	1.56 (br s)	15.9		12, 13, 15
15	1.96 (m)	40.4	16	12, 13, 14, 16
16	1.39[c]	26.8	15	17
17a	1.39[c]	37.5	16, 18	16
17b	1.31 (m)			16
18	2.75 (m)	31.8	19, 20	
19	1.06 (d, 7.0)	21.6	18	17, 18, 20
20	5.28 (d, 10.1)	115.9	18	17, 19, 21, 22
21		144.9		
22		164.2		
23		99.2		
24		173.3		
25	1.75 (s)	6.1		22, 23, 24
1′	4.22 (s)	44.3		1, 4, 2′
2′		172.3		

[a] ^{13}C assignments supported by HSQC experiment.
[b,c] Overlapping signals.

Table 2
NMR data (600 MHz, methanol-d_4) for 8-hydroxyircinialactam A (**5**)

#	δ_H (mult, J Hz)	δ_C[a]	COSY	HMBC (^1H–^{13}C)
1	4.06 (br s)	52.9	2, 5	2, 3
2	6.93 (br s)	138.6	1	1, 3, 4, 5
3		139.4		
4		174.3		
5	2.27 (br t, 7.3)	27.2	1, 6	2, 4, 6
6	1.62 (m)	23.1	5, 7	5
7	1.50 (m)	42.2	6	6
8		73.2		
9	1.14 (s)	26.7		7, 8, 10
10	1.45 (m)	42.7	11	8, 11
11	2.01 (m)	23.5	10, 12	10, 12, 13
12	5.13 (br t, 7.1)	126.0	11, 14	11, 14, 15
13		135.9		
14	1.58 (br s)	15.7		12, 13, 15
15	1.96 (br t, 7.0)	40.4	16	16
16	1.39[b]	26.7	15	17
17a	1.39[b]	37.5	17b	16
17b	1.31 (m)		17a	
18	2.75 (m)	31.8	19, 20	
19	1.06 (d, 6.7)	21.0	18	17, 18, 20
20	5.28 (d, 10.2)	115.7	18	17, 19, 21, 22
21		145.0		
22		164.6		
23		98.9		
24		173.5		
25	1.75 (s)	6.1		22, 23, 24
1′	4.22 (s)	44.3		1, 4, 2′
2′		172.6		

[a] ^{13}C assignments supported by HSQC experiment.
[b] Overlapping signals.

Table 3
NMR data (600 MHz, methanol-d_4) for ircinialactam C (**7**)

#	δ_H (mult, J Hz)	δ_C[a]	COSY	HMBC (^{1}H–^{13}C)
1	4.05 (s)	52.9	2	2
2	6.89 (br s)	138.7	1	1, 4, 5
3		[d]		
4		174.2		
5	2.30[b]	26.9		2, 6
6	2.27[b]	27.0	7	5, 7, 8
7	5.16 (br t, 6.6)	124.5	6	5, 9, 10
8		137.1		
9	1.61 (br s)	16.1		7, 8, 10
10	2.01 (br t, 7.9)	40.8	11	7, 8, 9, 11
11	2.09[c] (m)	27.6	10, 12	10, 12, 13
12	5.11 (br t, 6.6)	125.5	11	14, 15
13		136.0		
14	1.59 (br s)	15.9		12, 13, 15
15	1.97 (br t, 8.0)	40.7	16	12, 13, 14, 16, 17
16	1.44 (m)	26.3	15	
17a	1.31 (m)	37.5		
17b	1.17 (m)			
18	1.92 (m)	31.4	19, 20a	
19	0.94 (d, 5.7)	20.1	18	17, 18, 20
20a	2.27[b]	42.6	18, 20b	17, 18, 19, 21
20b	2.07[c]		20a	17, 18, 19, 21
21		177.0		
1′	4.22 (s)	44.3		1, 2′, 4
2′		172.9		

[a] ^{13}C assignments supported by HSQC experiment.
[b,c] Overlapping signals.
[d] Not observed.

structure. The isomeric metabolite *ent*-ircinialactam C (**8**) displayed identical NMR data (Table S5, Supplementary data) to **7**, with resonances diagnostic for configurations about $\Delta^{7,8}$ (C-9, δ_C 16.3, *E*) and $\Delta^{12,13}$ (C-14, δ_C 16.1, *E*), and for the glycinyl lactam regiochemistry (H-2, δ_H 6.88). Analysis of the complete 1D and 2D NMR data, and more significantly a +ve $[\alpha]_D$, supported the assigned structure.

(+)HRESIMS analysis of ircinialactam D (**9**) returned a pseudomolecular ion $[M+Na]^+$ consistent with a molecular formula ($C_{29}H_{45}NO_9$, Δmmu 0.3) requiring eight DBE, suggestive of a glycinyl lactam of **1** in which the tetronic acid moiety had undergone ring opening and rearrangement. Analysis of the NMR data (Table S6, Supplementary data) revealed diagnostic resonances for configurations about $\Delta^{7,8}$ (C-9, δ_C 16.1, *E*) and $\Delta^{12,13}$ (C-14, δ_C 16.0, *E*), and the glycinyl lactam regiochemistry (H-2, δ_H 6.89), as well as resonances for an ethyl ester (δ_H 4.19/4.22, m, $CO_2CH_2CH_3$; δ_H 1.29, t, $CO_2CH_2CH_3$; δ_C 176.6, $CO_2CH_2CH_3$) and a carboxylic acid (δ_C 175.2, CO_2H). Excellent correlations between NMR data for **9** and **7**, particularly across the C-1 to C-19 structure fragment, as well as **9** and published data for a known dimethyl ester analogue,[27] together with analysis of the complete 1D and 2D NMR data, supported the structure as shown. While the relative configurations at C-21 and C-23 were not resolved, an 18*S* configuration was assigned on the basis of the known co-metabolites (**1**–**3**) and biogenic considerations.

2.3. Bioassay

The metabolites **1**–**9** represent known and new examples of the 'variabilin' family of marine sponge sesterterpenes. To further broaden our structure–activity relationship (SAR) investigations we also had access to authentic samples of the marine sponge metabolites 7,8-dihydroisopalinurin (**10**)[23] from a *Psammocinia* sp. and cometin A (**11**)[29] from a *Spongia* sp. All compounds were screened against recombinant α1 and α3 GlyRs using whole cell patch-clamp electrophysiology. The standard electrophysiological protocol involved voltage-clamping α1 or α3 GlyR-expressing HEK293 cells at −40 mV and inducing an inward current flux by applying an EC_{20} glycine concentration (i.e., a concentration that activates 20% of the saturating glycine-gated current). For α1 and α3 GlyRs, this corresponded to glycine concentrations of 15 and 100 μM, respectively. Unless otherwise indicated, GlyRs were first activated with a 2 s pulse of glycine alone and then with the same concentration of glycine plus a defined concentration of test compound. Usually a 1 min period elapsed between successive glycine plus compound applications. Under these experimental conditions, the known sesterterpene tetronic acids **1** and **2** had no significant effect on either α1 or α3 GlyRs at concentrations up to 100 μM (Table 4). However, the 8-hydroxy analogue **3** produced potent potentiation of α1 GlyRs. Examples of the effects of increasing concentrations of **3** at the α1 GlyR are shown in Figure 1A, with an averaged dose–response presented in Figure 1B. As summarised in Table 4, this compound exhibited a mean EC_{50} of 1.2 ± 0.2 μM and a maximum potentiation magnitude of 215 ± 39% (both n = 3 cells). It is apparent that a slowly-developing inhibition can also be observed at concentrations >30 μM, although this was not quantified. In contrast, **3** potently inhibited α3 GlyRs with a mean IC_{50} of 7.0 ± 1.5 μM (n = 3). Given this subunit-specific activity, we also tested the effects of **3** on transiently expressed α2 GlyRs using conventional whole cell patch-clamp recording, as described previously.[12] Receptors were activated with an EC_{20} (50 μM) glycine concentration and **3** applied at a concentration of 10 μM. Averaged from six cells, we found that this resulted in weak inhibition, to 87 ± 2% of control current magnitude.

As summarised in Table 4, the glycinyl lactam analogue **4** was a moderate potentiator of α1 GlyRs, producing an enhancement of 140 ± 12% (n = 7) at a concentration of 100 μM. Analogue **4** was also a modest inhibitor of α3 GlyRs (Table 4). Combining structural features of **3** and **4**, the 8-hydroxy glycinyl lactam **5** had no significant effect on α3 GlyRs at concentrations up to 100 μM, but was an effective potentiator of α1 GlyRs, with potentiation being significant at 1 μM and reaching 217 ± 15% (n = 6) at 100 μM, the highest concentration tested. However, as the potentation did not saturate by 100 μM, an EC_{50} could not be measured. By contrast, the isomer **6** was an exceptionally strong potentiator of α1 GlyRs. Examples of the effects of increasing concentrations of **6** at the α1 GlyR are shown in Figure 2A, with an averaged dose–response presented

Table 4
Summary of the potentiation (EC_{50}) and antagonism (IC_{50}) of GlyRs

Compound	Potentiation		Antagonism	
	α1 GlyR EC_{50} (μM) MP (%)	α3 GlyR EC_{50} (μM) MP (%)	α1 GlyR IC_{50} (μM)	α3 GlyR IC_{50} (μM)
1	—	—	—	—
2	—	—	—	—
3	1.2 ± 0.2 215 ± 39	—	—	7.0 ± 1.5[a]
4	No saturation 140 ± 12	—	—	30–100
5	No saturation 217 ± 15	—	—	—
6	0.5 ± 0.3[b] 330 ± 28	No saturation 183 ± 19	—	—
7	—	—	—	30–100
8	—	—	—	30–100
9	—	—	—	30–100
10	—	—	—	—
11	—	—	—	—

MP = maximum potentiation expressed as a percentage of EC_{20} glycine current. A dash (—) indicates no activity was observed. No saturation = no current saturation was observed at drug concentrations up to 100 μM and hence EC_{50} values could not be calculated. All mean data were averaged from 3–7 cells.
[a] Hill coefficient (n_H) = 0.9 ± 0.15 μM.
[b] Hill coefficient (n_H) = 0.5 ± 0.3 μM.

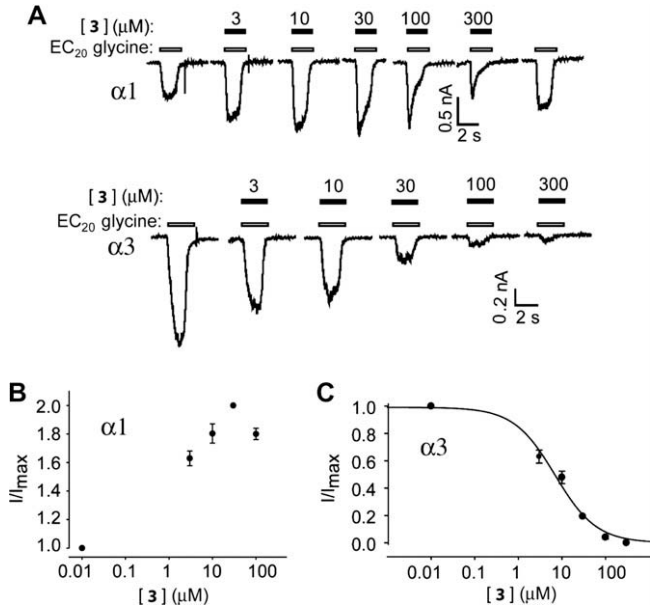

Figure 1. Effects of **3** on α1 and α3 GlyRs. (A) Effects of indicated concentrations of **3** on currents activated by EC_{20} glycine concentrations α1 and α3 GlyRs (upper and lower panels, respectively). Unfilled bars denote glycine applications and filled bars denote compound applications. (B) Averaged dose–response of **3** at α1 GlyRs ($n = 3$ cells). (C) Averaged dose–response of **3** at α3 GlyRs ($n = 3$ cells). Mean parameters of best fit to dose–response curves are given in the text.

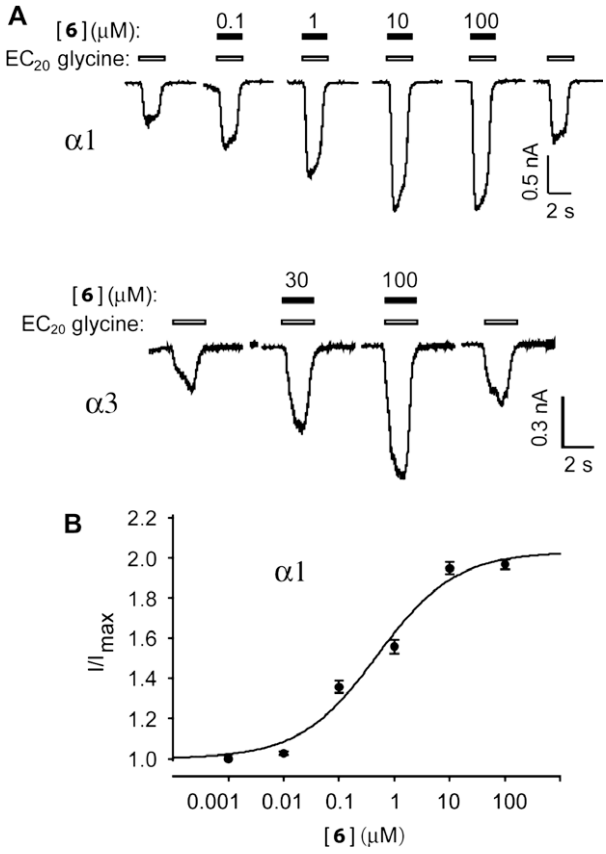

Figure 2. Effects of **6** on α1 and α3 GlyRs. (A) Effects of indicated concentrations of **6** on currents activated by EC_{20} glycine concentrations α1 and α3 GlyRs (upper and lower panels, respectively). Unfilled bars denote glycine applications and filled bars denote compound applications. (B) Averaged dose–response of **6** at α1 GlyRs ($n = 5$ cells). Mean parameters of best fit to dose–response curves are given in the text.

in Figure 2B. As summarised in Table 4, the dose–response was fitted with a mean EC_{50} of 0.5 ± 0.3 μM and a maximum potentiation magnitude of 330 ± 28% (both $n = 5$ cells). Compound **6** also potentiated α3 GlyRs with much weaker potency. The mean potentiation elicited by 100 μM of **6** was 183 ± 19% ($n = 6$). These data support the proposition that the 8-hydroxy and glycinyl lactam functionalities are key elements of the GlyR potentiating pharmacophore.

Negligible to at best modest antagonist activity (30–100 μM) associated with **7**–**9** highlights the significance of the conjugated tetronic acid moiety (Table 4). These observations on the pharmacophore are further confirmed by the absence of significant activity associated with **10**–**11**.

3. Discussion

Analogs **3**, **5** and **6** all modulated GlyRs in the sub-micromolar to low-micromolar range and exhibited differential effects on α1 and α3 GlyRs. Analog **3** exhibited the strongest subunit-specificity. At a 10 μM concentration, **3** strongly potentiated α1 GlyRs, had little effect on α2 GlyRs and potently inhibited α3. This is the first α3 specific inhibitor yet identified. Until now, the only compounds known to exhibit strong subunit-specific inhibition of GlyRs were the synthetic cannabinoids (HU-210, HU-308 and WIN-55,212-2). These compounds all inhibited both α2 and α3 GlyRs with affinities ranging from 50 nM to 1 μM, while having little or no inhibitory effect on α1 GlyRs up to 30 μM.[12] HU-210 did, however, produce strong potentiation of α1 GlyRs. Of course, the synthetic cannabinoids have numerous off-target actions that render them unsuitable as pharmacological probes or GlyR-targeted therapeutics. Provided **3** does not exhibit off-target actions, it may be useful as a pharmacological probe for identifying the presence of α3-containing GlyRs and for investigating their contribution to glycinergic signalling on spinal nociceptive sensory neurons. Due to its ability to selectively inhibit α3 GlyRs, **3** may also be a promising starting point for the development of lead compounds to treat temporal lobe epilepsy.[17,18]

Analogs **3**, **5** and **6** selectively and dramatically potentiated α1 GlyR currents at sub- to low-micromolar concentrations. As **5** and **6** had little effect on α3 GlyRs in this concentration range, they can thus be considered as α1 GlyR-specific potentiators. To date only a few α1 GlyR-specific potentiators have been identified. NV-31, a gingkolide derivative, exhibits an α1 GlyR-specific potentiating action at 1–10 μM, although the magnitude of its effect (135%) is small.[30] While some dihydropyridine and tropeine derivatives selectively potentiate α1 GlyRs over other GlyR subtypes,[31–35] both compound classes have well-known, clinically important effects on other ion channels. Finally, pregnenolone, an endogenous steroid, potentiates α1 but not α2 GlyRs in the 2–20 μM range,[36] although it has much higher potencies at GABA-A receptors.[37] Thus, all previously identified GlyR α1-specific potentiators have either weak activity or potent off-target actions. If **5** and **6** prove to be highly specific as α1 GlyR enhancers, they could be useful as therapeutic leads for movement disorders such as spasticity and hyperekplexia.[38]

Literature reports of novel natural products can prompt total syntheses targeting both the natural products themselves, and the structure class in general. In addition to developing valuable new methodology, synthetic studies are typically justified by the claim that an effective synthesis can be essential for supplying the material needed for pharmacological investigation. This claim is particularly accurate in the case of marine sponge metabolites, where recollection and resupply is often problematic or impossible, isolated yields are low, and poor stability can limit the duration of access to a particular metabolite, often precluding or at least curtailing biological assessment. The value of successful total

syntheses notwithstanding, choice of target is frequently driven by factors other than pharmacological imperative. In the absence of knowledge of its unique effect on GlyRs, it is hardly surprising that, despite being known for two decades, the sesterterpene tetronic acid **3** failed to attract the attention of synthetic chemists. Our findings reveal that sesterterpene tetronic acids, such as **3**, **5** and **6**, embody an exciting new pharmacophore worthy of synthetic attention. Future synthetic studies could provide a library of natural products and analogues for both in vitro and in vivo evaluation, defining the importance of the glycinyl lactam, 8-hydroxy and conjugated tetronic acid moieties to the pharmacophore, characterising requirements for subunit selectivity, and differentiating the molecular basis behind antagonism versus potentiation.

4. Conclusion

In this investigation, we successfully challenged a library of >2500 marine extracts to focus attention on three geographically distinct sponges of the Family Irciniidae that in turn yielded an array of sesterterpene tetronic acids, examples of which were shown to be potent subunit-selective GlyR modulators. The glycinyl lactam pharmacophore identified during this investigation may inspire the development of new pharmacological tools capable of probing the distribution and function of GlyR isoforms, potentially advancing the development of GlyR targeting therapeutics to treat chronic inflammatory pain, epilepsy, spasticity and/or hyperekplexia.

5. Experimental

5.1. Equipment

Chiroptical measurements ($[\alpha]_D$) were obtained on a JASCO P-1010 polarimeter in a 100 × 2 mm cell. UV spectra were acquired from a Cary 50 UV–vis spectrophotometer. NMR spectra were obtained on a Bruker Avance DRX600 spectrometer equipped with a 3 mm HPLC–SEI ^1H–^{13}C/D Z-GRD flow probe in the solvents indicated and referenced to residual ^1H signals in the deuterated solvents. HPLC–DAD–SPE was performed using an Agilent 1100 Series Separations Module equipped with a Bruker Diode Array Detector coupled to a Spark Prospekt2 SPE unit. All NMR data was acquired in methanol-d_4 unless otherwise specified. Electrospray ionisation mass spectra (ESIMS) were acquired using an Agilent 1100 Series separations module equipped with an Agilent 1100 Series LC/MSD mass detector in both positive and negative ion modes. High-resolution ESIMS measurements were obtained on a Bruker micrOTOF mass spectrometer by direct infusion in MeCN at 3 μL/min using sodium formate clusters as an internal calibrant. HPLC was performed using an Agilent 1100 Series separations module equipped with Agilent 1100 Series diode array and/or multiple wavelength detectors and Agilent 1100 Series fraction collector, controlled using ChemStation Rev.9.03A and Purify version A.1.2 software.

Fluorescence experiments were performed using an automated imaging system with a robot-controlled liquid handling system constructed in the laboratory. The 384-well plates were placed onto a motorised stage (Prior ProScan II, GT Vision, Hagerstown, MD, USA) of an Olympus IX51 inverted microscope and cells were imaged with an Olympus 10× objective (UPlanFLN, N.A. 0.30). Illumination to excite YFP fluorescence was provided by an Osram 100 W mercury short arc lamp (HBO 103/2), passing through an Olympus YFP dichroic mirror (86002V2 JP4 C76444). Emitted fluorescence passed through a magnifier lens (diopter 8, mineral glass), and was then imaged by a Photometrics CoolSNAP CF monochrome camera (Roper Scientific GmbH, Ottobrun, Germany) and digitised onto a personal computer. The final resolution of the images was 696 × 520 pixels. The maximum image acquisition rate used in these experiments was 1.25 Hz. Liquid-handling was performed with an LC PAL autosampler (CTC Analytics, Zwingen, Switzerland) using a 100-μL syringe. A suite of LabView 8.2.1 software (National Instruments Corp, Austin, Texas, USA) routines purpose-written in the laboratory were used for hardware control, image acquisition, storage, image analysis and data quantification. Whole cell patch-clamp recordings were performed using an automated planar patch-clamp device (Patchliner, Nanion Technologies GmbH, Munich, Germany).

5.2. Marine extracts library

A library of >2500 marine invertebrate and alga samples, collected from locations across southern Australia and Antarctica, including intertidal, coastal and deep sea locations, were acquired (Capon) over a period of 25+ years. Individual samples were documented, diced and steeped in EtOH at −30 °C for prolonged storage. A portion (7 mL) of each EtOH extract was decanted into a labelled, tared screw cap vial (8 mL) and the solvent evaporated in vacuo. The residue was weighed (25–50 mg) and partitioned in situ by addition of *n*-BuOH (2 mL) and H_2O (2 mL). Typically, the biomass partitioned 10–20% into *n*-BuOH and 80–90% into H_2O. Aliquots (1 mL) of both *n*-BuOH and H_2O phases were transferred to deep 96-well plates, to generate a set of extract library plates. These plates were subsequently used to prepare 10- and 100-fold dilution plates. The full set of extract and dilution plates represented a resource to support screening programs against a diverse array of bioassays.

For the initial screening, an aliquot (90 μL) of each 100-fold diluted *n*-BuOH partition was transferred into 384-well plates and each well was dried under a stream of nitrogen. The plates were stored at −30 °C, protected from light, until required. On the day of the assay, Ringer buffer (30 μL) was added to each well of the plates and an aliquot (10 μL) of each solution was transferred onto cells pre-incubated in Ringer buffer (15 μL). Assays were performed in horizontal duplicate. For the hit confirmation, an aliquot (24 μL) of each 10-fold diluted *n*-BuOH partition was transferred into 384-well plates, which were dried and stored as described previously. On the day of the assay, extracts were resuspended in Ringer buffer (80 μL) and aliquots (17 or 10 μL) were then transferred in horizontal duplicate onto cells pre-incubated in Ringer buffer (15 μL). The concentration dependence assisted in ranking extract potency for later prioritisation. Isolated pure compounds were prepared as 100 mM DMSO stock solution (10 μL), and were tested with patch-clamp at concentrations ranging from 10–300 μM final.

5.3. Extraction and isolation

A portion of the aqueous EtOH extract of specimen CMB-01064 (genus *Ircinia*; Museum Victoria Registry Number MVF 166265) was decanted and concentrated in vacuo, and the residue (2.25 g) partitioned between H_2O and *n*-BuOH. The *n*-BuOH soluble fraction was concentrated in vacuo (876.0 mg) and the residue was further triturated with light petroleum (19.9 mg), DCM (473.7 mg), MeOH (343.4 mg) and water (25.5 mg). A portion of the DCM soluble fraction (60.0 mg) was subjected to HPLC fractionation (Zorbax C_{18}, 5 μm 250 × 9.4 mm column, 4 mL/min gradient elution, 10–100% MeCN/H_2O with isocratic 0.01% TFA modifier) over 25 min to yield a mixture of **1** and **2** (6.5 mg, 5.9%), **3** (2.1 mg, 1.9%), **4** (4.0 mg, 3.6%), **5** (3.2 mg, 2.9%) and **6** (1.3 mg, 1.2%) (Scheme S1, Supplementary data). Yields calculated as a percentage of *n*-BuOH soluble fraction.

A portion of the aqueous EtOH extract of specimen CMB-03363 (genus *Ircinia*; Museum Victoria Registry Number MVF 166224) was decanted and concentrated in vacuo, and the residue (1.68 g) was partitioned between H_2O and *n*-BuOH. The *n*-BuOH soluble fraction was concentrated in vacuo (526.9 mg) and the residue further triturated with light petroleum (8.4 mg), DCM (267.8 mg), MeOH (208.1 mg) and water (41.4 mg) soluble. The DCM soluble fraction was subjected to HPLC (Zorbax C_8, 5 μm, 250 × 9.4 mm column, 4 mL/min gradient elution, 10–100% MeCN/H_2O with isocratic 0.01% TFA modifier over 25 min) to yield three fractions (I–III). Fraction II was essentially pure and was identified as **3** (10.0 mg, 1.9%). HPLC separation of a portion (3.2 mg) of fraction III (Zorbax C_3, 5 μm, 150 × 4.6 mm column, 1 mL/min gradient elution 50–100% MeCN/H_2O with isocratic 0.01% TFA modifier over 25 min) yielded **1** (1.2 mg, 3.7%) and **2** (1.4 mg, 4.4%). HPLC separation of fraction I (Zorbax C_8, 5 μm, 150 × 4.6 mm column, 1 mL/min gradient elution 10–100% MeCN/H_2O with isocratic 0.01% TFA modifier over 25 min) yielded **4** (0.3 mg 0.057%), **5** (0.2 mg, 0.037%), **7** (0.3 mg, 0.057%) and **9** (0.3 mg, 0.057%) (Scheme S2, Supplementary data). Yields calculated as a percentage of *n*-BuOH soluble fraction.

A portion of the EtOH extract of the third specimen, CMB-03231 (genus *Psammocinia*; Museum Victoria Registry Number MVF 166220), was also decanted and concentrated in vacuo and the residue (238.1 mg) was partitioned between H_2O and *n*-BuOH. The *n*-BuOH soluble fraction was concentrated in vacuo and the residue (124.8 mg) triturated with petroleum (1.4 mg), DCM (75.3 mg) and MeOH (43.4 mg). The DCM soluble fraction was subjected to HPLC fractionation (Zorbax C_8, 5 μm, 250 × 9.4 mm column, 4 mL/min gradient elution, 10–100% MeCN/H_2O with isocratic 0.01% TFA modifier over 25 min) yielded **8** (0.7 mg, 0.6%) (Scheme S3, Supplementary data). Yields calculated as a percentage of *n*-BuOH soluble fraction.

5.4. Characterisation of compounds

5.4.1. (7*E*,12*E*,20*Z*,18*S*)-Variabilin (1)

Colourless oil. $[\alpha]_D$ −24.8 (*c* 0.06, MeOH); UV–vis (MeOH) λ_{max} (log ϵ) 203 (4.27), 257 (3.93) nm; NMR data see Supplementary data Table S1; (+)HRESIMS *m/z* 421.2356 (calcd for $C_{25}H_{34}O_4Na$ 421.2349).

5.4.2. (7*E*,12*Z*,20*Z*,18*S*)-Variabilin (2)

Colourless oil. $[\alpha]_D$ −27.1 (*c* 0.05, MeOH); UV–vis (MeOH) λ_{max} (log ϵ) 202 (4.19), 249 (3.98), 308 (3.74) nm; NMR data see Supplementary data Table S2; (+)HRESIMS *m/z* 421.2356 (calcd for $C_{25}H_{34}O_4Na$ 421.2349).

5.4.3. (12*E*,20*Z*,18*S*)-8-Hydroxyvariabilin (3)

Colourless oil. $[\alpha]_D$ −37.4 (*c* 0.34, MeOH); UV–vis (MeOH) λ_{max} (log ϵ) 203 (4.33), 253 (4.27) nm; NMR data see Supplementary data Table S3; (+)HRESIMS *m/z* 439.2462 (calcd for $C_{25}H_{36}O_5Na$ 439.2455).

5.4.4. Ircinialactam A (4)

Colourless oil. $[\alpha]_D$ −20.5 (*c* 0.03, MeOH); UV–vis (MeOH) λ_{max} (log ϵ) 203 (4.40), 250 (4.14) nm; NMR data see Table 1; (+)HRESIMS *m/z* 494.2508 (calcd for $C_{27}H_{37}NO_6Na$ 494.2513).

5.4.5. 8-Hydroxyircinialactam A (5)

Colourless oil. $[\alpha]_D$ −19.5 (*c* 0.02, MeOH); UV–vis (MeOH) λ_{max} (log ϵ) 203 (4.33) nm; NMR data see Table 2; (+)HRESIMS *m/z* 512.2626 (calcd for $C_{27}H_{39}NO_7Na$ 512.2632).

5.4.6. 8-Hydroxyircinialactam B (6)

Colourless oil. $[\alpha]_D$ −12.0 (*c* 0.02, MeOH); UV–vis (MeOH) λ_{max} (log ϵ) 202 (4.40) nm; NMR data see Supplementary data Table S4; (+)HRESIMS *m/z* 512.2630 (calcd for $C_{27}H_{39}NO_7Na$ 512.2632).

5.4.7. Ircinialactam C (7)

Colourless oil. $[\alpha]_D$ −30.8 (*c* 0.03, MeOH); UV–vis (MeOH) λ_{max} (log ϵ) 203 (4.27) nm; NMR data see Table 3; (+)HRESIMS *m/z* 428.2413 (calcd for $C_{23}H_{35}NO_5Na$ 428.2407).

5.4.8. *ent*-Ircinialactam C (8)

Colourless oil. $[\alpha]_D$ +28.3 (*c* 0.03, MeOH); UV–vis (MeOH) λ_{max} (log ϵ) 201 (4.33) nm; NMR data see Supplementary data Table S5; (+)HRESIMS *m/z* 428.2404 (calcd for $C_{23}H_{35}NO_5Na$ 428.2407).

5.4.9. Ircinialactam D (9)

Colourless oil. $[\alpha]_D$ −19.9 (*c* 0.03, MeOH); UV–vis (MeOH) λ_{max} (log ϵ) 203 (4.48) nm; NMR data see Supplementary data Table S6; (+)HRESIMS *m/z* 574.2990 (calcd for $C_{29}H_{45}NO_9Na$ 574.2987).

5.4.10. 7,8-Dihydroisopalinurin (10)

Colourless oil. $[\alpha]_D$ +9.9 (*c* 0.09, MeOH); UV–vis (MeOH) λ_{max} (log ϵ) 204 (4.20) nm; NMR data see Supplementary data Table S7; (+)HRESIMS *m/z* 423.2507 (calcd for $C_{25}H_{36}O_4Na$ 423.2506).

5.4.11. Cometin A (11)

Colourless oil. $[\alpha]_D$ −11.5 (*c* 0.05, $CHCl_3$); UV–vis (EtOH) λ_{max} (log ϵ) 240 (3.85) nm; (+)HRESIMS *m/z* 433.1988 (calcd for $C_{25}H_{30}O_5Na$ 433.1985). NMR data consistent with published data.[29]

5.5. GlyR Bioassay

The first round of screening of marine extracts was performed using a YFP-based anion flux assay as described in detail previously.[39] Briefly, the cDNAs for YFP-I152L[40] and the human α1, α2 and α3L GlyR were subcloned separately into the pcDNA3.1 plasmid vector. HEK293 cells were transfected with the cDNAs for YFP-I152L plus one of the GlyR cDNAs using a calcium phosphate precipitation method. After termination of this procedure, cells were plated into wells of a 384-well plate at a density of around 3000 cells per well. Experiments were performed 24–48 h later. Around an hour before experiments, the culture medium in each well was replaced by 15 μL of Na gluconate solution containing (in mM): Na gluconate 140, KCl 5, $CaCl_2$ 2, $MgCl_2$ 1, HEPES 10, glucose 10, pH 7.3/NaOH. An aliquot (10 μL) of each fraction (containing 300 μg/mL dried material) was added to each well 30–45 min before experiments were commenced. Individual fractions were tested in duplicate. The experiments were performed using an automated imaging system with a robot-controlled liquid handling system constructed in the laboratory. The experimental protocol involved adding 50 μL of NaI solution (containing (in mM): NaI 140, KCl 5, $CaCl_2$ 2, $MgCl_2$ 1, HEPES 10, glucose 10, pH 7.3/NaOH) + 1 mM glycine to cells in each well to yield a final glycine concentration of ~670 μM. The chloride-induced fluorescence change was monitored 5–10 s later. Typically, 100–200 fluorescent GlyR-expressing cells were imaged per well. Fractions producing significant changes to either the resting or glycine-stimulated fluorescence levels were re-tested to confirm activity.

5.6. Generation of stably-expressing HEK293 cell lines

The human α1 and α3L GlyR subunit cDNAs in the pcDNA3.1 plasmid vector were linearized using ScaI and transfected into HEK293 cells using a calcium phosphate method and then maintained for 10–14 days in selection medium containing 1 mg/mL

G-418 and 10 μM strychnine for α1 GlyR and 500 μg/mL G-418 for α3 GlyR cell lines. From thenceforth, the two respective cell lines were always cultured in these selective media. Surviving transfected colonies were isolated and grown in the same media in 96-well plate for two weeks. Any large monoclonal colonies were screened for functional response to 10 mM glycine using the YFP-based chloride flux assay described above. In these experiments, several clones of either α1 or α3 GlyRs that exhibited a significant fluorescence quench to glycine exposure were identified and one clonal cell line of each subunit was selected for further characterisation using both patch-clamp and YFP assays.

5.7. Electrophysiology

We employed a Nanion Patchliner automated planar chip patch-clamp device (NPC-16A, Nanion Technologies GmbH, Munich, Germany) to perform whole cell recordings on up to 8 cells simultaneously. In addition to increasing throughput, this device permits complete exchange of the solution bathing the cells with 25 μL of new solution. For Patchliner experiments, the stable α1 and α3 GlyR-HEK293 cells were suspended in the standard external solution containing (in mM): 140 NaCl, 4 KCl, 2 $CaCl_2$, 1 $MgCl_2$, 10 HEPES/NaOH and 5 glucose (pH 7.4) at a density of 1×10^6–5×10^7 cells/mL. The cell suspension, the pre-prepared internal solution [(in mM) 50 KCl, 10 NaCl, 60 KF, 2 $MgCl_2$, 10 HEPES/KOH (pH 7.2), and 20 EGTA], the external solution and the compound-containing solutions are all placed at pre-defined positions on the workstation and were applied to cells via robotic control. For dose–response experiments, cells were voltage-clamped at −40 mV at room temperature (20–24 °C). Compounds to be tested were dissolved in DMSO and kept at −20 °C, with solutions for experiments prepared from these stocks on the day of recording.

Results are expressed as mean ± SEM of three or more independent experiments. The Hill equation was used to calculate the half-maximal concentration (EC_{50}) and Hill coefficient (n_H) values for activation. A similar equation was also used to calculate the half-maximal concentrations for inhibition (IC_{50}) and n_H values for inhibition. All curves were fitted using a non-linear least squares algorithm (Sigmaplot 9.0, Jandel Scientific). Statistical significance was determined by unpaired Student's *t*-test with $P < 0.05$ representing significance.

Acknowledgements

We thank L. Goudie (Museum Victoria) for taxonomic analysis and S. Nevin for help with the Patchliner. W.B. was supported by an Australian Development Scholarship and J.W.L. was supported by a fellowship from the National Health and Medical Research Council of Australia. We also acknowledge the support of the Australian Research Council Special Research Centre for Functional and Applied Genomics, the Institute for Molecular Bioscience and The University of Queensland.

Supplementary data

Supplementary data associated with this article can be found, in the online version, at doi:10.1016/j.bmc.2010.03.002.

References and notes

1. Lynch, J. W. *Physiol. Rev.* **2004**, *84*, 1051.
2. Jeong, H. J.; Jang, I. S.; Moorhouse, A. J.; Akaike, N. *J. Physiol.* **2003**, *550*, 373.
3. Turecek, R.; Trussell, L. O. *Nature* **2001**, *411*, 587.
4. Ye, J. H.; Wang, F.; Krnjevic, K.; Wang, W.; Xiong, Z. G.; Zhang, J. *J. Neurosci.* **2004**, *24*, 8961.
5. Betz, H.; Laube, B. *J. Neurochem.* **2006**, *97*, 1600.
6. Harvey, R. J.; Depner, U. B.; Wassle, H.; Ahmadi, S.; Heindl, C.; Reinold, H.; Smart, T. G.; Harvey, K.; Schutz, B.; Abo-Salem, O. M.; Zimmer, A.; Poisbeau, P.; Welzl, H.; Wolfer, D. P.; Betz, H.; Zeilhofer, H. U.; Muller, U. *Science* **2004**, *304*, 884.
7. Haverkamp, S.; Muller, U.; Harvey, K.; Harvey, R. J.; Betz, H.; Wassle, H. *J. Comp. Neurol.* **2003**, *465*, 524.
8. Haverkamp, S.; Muller, U.; Zeilhofer, H. U.; Harvey, R. J.; Wassle, H. *J. Comp. Neurol.* **2004**, *477*, 399.
9. Heinze, L.; Harvey, R. J.; Haverkamp, S.; Wassle, H. *J. Comp. Neurol.* **2007**, *500*, 693.
10. Webb, T. I.; Lynch, J. W. *Curr. Pharm. Des.* **2007**, *13*, 2350.
11. Lynch, J. W. *Neuropharmacology* **2009**, *56*, 303.
12. Yang, Z.; Aubrey, K. R.; Alroy, I.; Harvey, R. J.; Vandenberg, R. J.; Lynch, J. W. *Biochem. Pharmacol.* **2008**, *76*, 1014.
13. Zeilhofer, H. U. *Rev. Physiol. Biochem. Pharmacol.* **2005**, *154*, 73.
14. Zeilhofer, H. U. *Cell. Mol. Life Sci.* **2005**, *62*, 2027.
15. Froh, M.; Thurman, R. G.; Wheeler, M. D. *Am. J. Physiol. Gastrointest. Liver. Physiol.* **2002**, *283*, G856.
16. Gundersen, R. Y.; Vaagenes, P.; Breivik, T.; Fonnum, F.; Opstad, P. K. *Acta Anaesthesiol. Scand.* **2005**, *50*, 1108.
17. Eichler, S. A.; Kirischuk, S.; Jüttner, R.; Schafermeier, P. K.; Legendre, P.; Lehmann, T. N.; Gloveli, T.; Grantyn, R.; Meier, J. C. *J. Cell Mol. Med.* **2008**, *12*, 2848.
18. Eichler, S. A.; Förstera, B.; Smolinsky, B.; Jüttner, R.; Lehmann, T. N.; Fähling, M.; Schwarz, G.; Legendre, P.; Meier, J. C. *Eur. J. Neurosci.* **2009**, *30*, 1077.
19. Faulkner, D. J. *Tetrahedron Lett.* **1973**, *39*, 3821.
20. Capon, R. J.; Dargaville, T. R.; Davis, R. *Nat. Prod. Lett.* **1994**, *41*, 51.
21. Holler, U.; Konig, G. M.; Wright, A. D. *J. Nat. Prod.* **1997**, *60*, 832.
22. Barrow, C. J.; Blunt, J. W.; Munro, M. H. G.; Perry, N. B. *J. Nat. Prod.* **1988**, *51*, 275.
23. Murray, L.; Hamit, H.; Hooper, J. N. A.; Hobbs, L.; Capon, R. J. *Aust. J. Chem.* **1995**, *48*, 1899.
24. Martinez, A.; Duque, C.; Sato, N.; Tanaka, R.; Fujimoto, Y. *Nat. Prod. Lett.* **1995**, *6*, 1.
25. Shin, J.; Rho, J.-R.; Seo, Y.; Lee, H.-S.; Cho, K. W.; Sim, C. J. *Tetrahedron Lett.* **2001**, *42*, 3005.
26. Liu, Y. H.; Mansoor, T. A.; Hong, J. K.; Lee, C. O.; Sim, C. J.; Im, K. S.; Kim, N. D.; Jung, J. H. *J. Nat. Prod.* **2003**, *66*, 1451.
27. Wang, N.; Song, J.; Jang, K. H.; Lee, H. S.; Li, X.; Oh, K. B.; Shin, J. *J. Nat. Prod.* **2008**, *71*, 551.
28. Gonzalez, A. G.; Rodriguez, M. L.; Barrientos, A. S. *J. Nat. Prod.* **1983**, *46*, 256.
29. Urban, S.; Capon, R. J. *Aust. J. Chem.* **1992**, *45*, 1255.
30. Lynch, J. W.; Chen, X. *Neurosci. Lett.* **2008**, *435*, 147.
31. Supplisson, S.; Chesnoy-Marchais, D. *Mol. Pharmacol.* **2000**, *58*, 763.
32. Yang, Z.; Ney, A.; Cromer, B. A.; Ng, H. L.; Parker, M. W.; Lynch, J. W. *J. Neurochem.* **2007**, *100*, 758.
33. Chesnoy-Marchais, D.; Cathala, L. *Eur. J. Neurosci.* **2001**, *13*, 2195.
34. Chen, X.; Cromer, B.; Webb, T. I.; Yang, Z.; Hantke, J.; Harvey, R. J.; Parker, M. W.; Lynch, J. W. *Neuropharmacology* **2009**, *56*, 318.
35. Maksay, G.; Laube, B.; Schemm, R.; Grudzinska, J.; Drwal, M.; Betz, H. *J. Neurochem.* **2009**, *109*, 1725.
36. Maksay, G.; Laube, B.; Betz, H. *Neuropharmacology* **2001**, *41*, 369.
37. Lambert, J. J.; Cooper, M. A.; Simmons, R. D.; Weir, C. J.; Belelli, D. *Psychoneuroendocrinology* **2009**, *34*, S48.
38. Laube, B.; Maksay, G.; Schemm, R.; Betz, H. *Trends Pharmacol. Sci.* **2002**, *23*, 519.
39. Kruger, W.; Gilbert, D.; Hawthorne, R.; Hryciw, D. H.; Frings, S.; Poronnik, P.; Lynch, J. W. *Neurosci. Lett.* **2005**, *380*, 340.
40. Galietta, L. J.; Haggie, P. M.; Verkman, A. S. *FEBS Lett.* **2001**, *499*, 220.